Carbohydrate Polymer Technologies and Applications 2 (2021) 100136

Contents lists available at ScienceDirect

Carbohydrate Polymer Technologies and Applications

journal homepage: www.sciencedirect.com/journal/carbohydrate-polymer-technologies-and-applications

Xyloglucan and Concanavalin A based dressings in the topical treatment of mice wound healing process

Isabel R.S. Arruda [a], Marthyna P. Souza [a,*], Paulo A.G. Soares [a], Priscilla B.S. Albuquerque [b], Túlio D. Silva [a], Paloma L. Medeiros [c], Marcia V. Silva [a], Maria T.S. Correia [a], António A. Vicente [e], Maria G. Carneiro-da-Cunha [a,d,*]

[a] Departamento de Bioquímica, Universidade Federal de Pernambuco, Av. Prof. Moraes Rego s/n, CEP: 50.670-420 Recife, PE, Brasil
[b] Departamento de Medicina, Universidade de Pernambuco, campus Garanhuns, R. Cap. Pedro Rodrigues, São José, Garanhuns, Pernambuco CEP 55294-902, Brazil
[c] Departamento de Histologia e Embriologia, Universidade Federal de Pernambuco, Av. Prof. Moraes Rego s/n, CEP: 50.670-420 Recife, PE, Brasil
[d] Laboratório de Imunopatologia Keizo Asami-LIKA, Universidade Federal de Pernambuco, Av. Prof. Moraes Rego s/n, CEP: 50.670-420 Recife, PE, Brasil
[e] IBB–Institute for Biotechnology and Bioengineering, Centre of Biological Engineering, Universidade do Minho, Campus de Gualtar, 4710-057 Braga, Portugal

ARTICLE INFO

Keywords:
Polysaccharide films
Hymenaea courbaril
Film characterization
Wound healing
Serum proteome

ABSTRACT

For medical biomaterials, xyloglucan dispersions can form films or gels to be applied as a wound dressing. For this purpose, the structural characterization of xyloglucan dressing (XG) and xyloglucan dressing containing 0.5 mg/mL of concanavalin A (XGL) was performed. The lectin release capacity and stability, cytotoxicity, and pro-wound healing effects were also investigated. XG and XGL films were prepared by mixing 0.5 % (w/v) xyloglucan with 0.3 % (v/v) glycerol. The ConA incorporated in the xyloglucan dressing maintained its biological activity for fourteen days in a controlled-release manner. The films were non-toxic, homogeneous, flexible, and accelerated the wound contraction compared with the control group, promoting less infiltration of inflammatory cells, angiogenesis, remodeling, and early epithelization. The films also alleviate the inflammation phase by reducing the production of pro-inflammatory cytokines (IFN-γ, TNF-α, IL-1β, IL-6, and IL-12), especially the XGL film, which promoted the up- and down-regulation of important proteins associated with the wound repair. All these findings suggest that XG and XGL films may represent a good therapeutic approach for wound healing applications.

1. Introduction

The wound healing process takes place to restore the anatomical and functional integrity of the tissue after a physical or thermal wound. For this, the organism makes use of a sequence of biochemical and cellular events in response to tissue damage. These events are divided into the following phases: inflammatory, proliferation or granulation of the extracellular matrix (ECM), and ECM remodeling for scar formation (Kordestani, 2019). In this process, time is an important aspect and researchers in this field are looking-for the development of new products and therapies that can accelerate the healing and given a better quality to the healed skin (Ajith et al., 2021; Picone et al., 2019).

Xyloglucans (XG) from the primary cell walls of monocotyledons seeds (*Tamarindus indica, Copaifera langsdorffii*, and *Hymenaea courbaril*) (Hayashi & Kaida, 2011) are high molecular weight neutral branched polysaccharides. Its chemical structure has a cellulose-like backbone, composed of β-glucosyl ring units with ribbon-like conformation, where single units of xylose and galactose substituents form a part of the branches (Nishinari et al., 2021). Here we have used the XG (≥ 500 kDa) from *Hymenaea courbaril* var. *courbaril* seeds with a central backbone composed by 4-linked β-glucose branched at position 6 with non-reducing terminal units of α-xylose or β-galactose-(1→2)-α-xylose disaccharides (Arruda et al., 2015). Xyloglucans from different sources were extensively used in the production of biomaterials, especially in pharmaceuticals, as drug delivery devices (Farias et al., 2018; Kulkarni et al., 2017; Pardeshi et al., 2018). In addition, it was reported that this polymer has anti-inflammatory and immunomodulatory properties and synergistic effects with other anti-inflammatory biomolecules when used in topical and mucosal wound dressings (Zhou et al., 2020).

Lectins are proteins and glycoproteins which could bind to specific

* Corresponding authors at: Departamento de Bioquímica, Universidade Federal de Pernambuco-UFPE, Av. Prof. Moraes Rego, S/N, Cidade Universitária, CEP 50.670-420 Recife, PE, Brasil.
E-mail addresses: marthynapessoa2@gmail.com.br (M.P. Souza), mgcc@ufpe.br (M.G. Carneiro-da-Cunha).

https://doi.org/10.1016/j.carpta.2021.100136
Received 27 May 2021; Received in revised form 23 July 2021; Accepted 9 August 2021
Available online 10 August 2021

monomers either a soluble carbohydrate or the carbohydrate portion of a glycoconjugate. These interconnective proteins are present in both plants and animals and play roles in various biological processes, including immunomodulation and cell adhesion (Coelho et al., 2017; Santos et al., 2014). Concanavalin A (ConA), a lectin from *Canavalia ensiformis* seeds, possess immunomodulatory effects as a mitogenic agent for lymphocytes cell, activating the nuclear factor of activated T cells, an important transcription factors in the activation of immune system (Bemer & Truffa-Bachi, 1996; Dwyer & Johnson, 1981).

The advances in tissue engineering and regenerative medicine has transformed the wound care world into advanced technological matrices that not only prevent infections, but also improve the process of dermal and epidermal tissue recovery, in addition to modulate the expression of growth factors involved in the healing process (Ajith et al., 2021). Polysaccharides are the most explored natural polymers in the preparation of biomaterials for wound care. For example, cellulose (Liu et al., 2020), chitosan (Shivakumar et al., 2021), and galactomannans (Albuquerque et al., 2017; Yadav & Maiti, 2020), have been extremely explored in the development of intelligent wound dressings; however, XG based matrix reported so far are few (Ajovalasit et al., 2018a; Ajovalasit et al., 2018b; Andrade et al., 2021; Picone et al., 2019).

The immobilization of ConA into XG, sodium alginate, and galactomannan membranes was previously reported in the development of biosensors for Dengue viruses antigens (Pereira et al., 2008; Valenga et al., 2012). In what concerns the best of our knowledge, there are no previous reports on XG/ConA based wound dressings; its application in wound care, the characterization of the dressing, and its influence on the healing process is also unknown and constitutes an important goal for exploration in the biomedical and medical fields.

This study aimed at the production and the structural and bioactive characterization of xyloglucan membranes obtained from *H. courbaril* seeds with or without the incorporation of ConA. For this, an extensive study was performed in which we evaluated the profile of the drug release, the stability and cytotoxicity of the films, and their ability to improve the quality of the new tissue formed on experimental wounds in mice.

2. Material and methods

2.1. Wound dressing preparation

The XG (81±7 % of purity, MW≥ 500 kDa, with a central backbone composed by 4-linked β-glucose branched at position 6 with non-reducing terminal units of α-xylose or β-galactose-(1→2)-α-xylose disaccharides) contained in *Hymenaea courbaril* var. *courbaril* seeds was obtained according to Arruda et al. (2015).

The wound dressings were prepared by mixing (200 rpm) a XG solution (0.5% w/v) with glycerol 0.3% (v/v) for two hours at 25°C. The pH was adjusted to 5.8 with 1.0 M NaOH solution. Commercial concanavalin A (ConA from Sigma Aldrich, USA), ConA conjugated with fluorescein isothiocyanate (ConA-FITC), and ConA conjugated with gold (ConA-Au) were prepared at 0.5 mg/mL concentration. After, each protein was mixed (200 rpm) with the XG solution at 25°C for 30 min. The concentration of ConA incorporated into the filmogenic solution was based on the study carried out by Andrade et al. (2021), where the incorporation of the *Cratylia mollis* lectin (Cramoll) into a xyloglucan matrix was performed; considering that Cramoll is a glucose/mannose specific lectin, as well as ConA, we used the same concentration reported in the literature. Afterwards, 15 mL of each filmogenic solution were placed in acrylic plates (90 mm × 15 mm) and dried at 37 °C for 24 h. Dried wound dressings, named Xyloglucan (XG), Xyloglucan-ConA (XGL), Xyloglucan-ConA-FITC (XGL-FITC), and Xyloglucan-ConA-Au (XGL-Au) were stored in desiccators at 25°C and 54.0% of relative humidity (maintained by $Mg(NO_3)_2.6H_2O$ saturated solution) until further analysis.

2.2. Characterization of the wound dressings

FTIR spectra of XG and XGL were obtained by infrared spectrometer (VERTEX 70, Bruker Optics, USA), using Attenuated Total Reflectance (ATR) mode. The analysis conditions for scanning the spectra were 4 cm^{-1} of resolution, co-adding 128 scans, and frequency range 4000–500 cm^{-1}.

The fluorescent pattern of XGL-FITC was evaluated by green fluorescence mode using a DMI 4000 B fluorescence microscope (Leica Microsystems, Wetzlar, Germany). The band-pass and the long-pass (488 nm) filters were used respectively to excite and to collect the fluorescence, allowing the visualization of the lectin incorporated into the xyloglucan wound dressing. All images were acquired with a color Pixelfly camera (PCO-TECH Inc., Romulus, MI, USA). The analysis of the morphology and microstructure of XGL-Au, immobilized on copper grids, was observed by a transmission electron microscopy (FEI Morgagni 268D 40-100kV, PHILIPS, EUA).

The measurements of the water vapor permeability (WVP) were carried out gravimetrically as described by Souza et al. (2015). Oxygen permeability (O_2P) was determined based on the ASTM D 3985-17 (ASTM, 2017). Tensile strength (TS) and elongation-at-break (EB) were measured with an Instron Universal Testing Machine (Model 4500, Instron Corporation, USA) according to the ASTM D882-10 (ASTM 2010). Three measurements were obtained for each sample.

2.3. In vitro assessment of ConA release, bioactive stability, and cytotoxicity of the dressings

The bioactivity of ConA lectin was evaluated by the Hemagglutination Activity (HA) assay, which was defined as the lowest lectin dilution that showed complete hemagglutination of rabbit blood cells (Correia & Coelho, 1995). Samples of XG and XGL were solubilized in NaCl 0.9 % until reach a final ConA concentration of 0.0 and 0.5 mg/mL, respectively. Free ConA (0.5 mg/mL) was used as standard.

The ConA release assay was performed by incubating XGL into 15 mL of Citrate-Phosphate Buffer solution 0,1 M, pH 6.0 for 96 h. At certain time intervals, 1.0 mL of samples were taken from the buffer solution and 1.0 mL of fresh buffer were added to the system to keep the volume of release medium constant. The samples were evaluated by HA and protein concentration (Bradford, 1976).

To assess the mechanism of ConA release, experimental data were fitted to four specific kinetic models (Souza et al., 2015; Korsmeyer & Peppas, 1981):

$$\text{Zero order}: Q_t = Q_0 + K_0 t \quad (1)$$

$$\text{First order}: InQ_t = InQ_0 + K_1 t \quad (2)$$

$$\text{Higuchi}: Q_t = K_H t^{1/2} \quad (3)$$

$$\text{Korsmeyer} - \text{Peppas}: Q_t = K_k t^n \quad (4)$$

where: Q_t is the amount of ConA released over time; Q_0 is the amount of ConA released at time 0; K_0, K_1, K_H e K_k are kinetic constants and n is the release exponent.

The stability of XGL during 97 days of storage was determined by evaluating the HA of the wound dressing at 4 and 30°C. In determinate times between 0 and 97 days, samples of XGL at each temperature of storage were solubilized in 15 mL NaCl 0.9% and submitted to HA evaluation. ConA at 0.5 mg/mL concentration was used as positive control of the HA assay.

To determine the nontoxic concentration of XG e XGL, splenocytes from BALB/c mice (6×10^5 cells/well) were cultured in ninety-six well plate in RPMI 1640 media supplemented with 10.0% fetal bovine serum and 50 μg/mL of gentamycin. Cells were incubated in the presence of ^{3}H-thymidine during 24 h at 37°C and 5.0% CO_2. According to the

treatment, cells were grouped on: treated with dissolved XG and XGL dressings in RPMI media (1, 5, 10, 25, 50, and 100 μg/mL), negative control group (cells incubated with ^{3}H-thymidine), and positive control group (cells treated with saponin and incubated with ^{3}H-thymidine). After 24 h, the cultures were harvested using a cell harvester to determine the ^{3}H-thymidine incorporation in a beta radiation counter. The viability of the cells was determined by the incorporation of ^{3}H-thymidine in XG and XGL treatments, and the 50% cytotoxic concentration (CC_{50}) was defined as the wound dressing concentration that reduced 50% of viable cells when compared with the negative control (Pereira et al., 2004).

2.4. In vivo wound healing study

Male BALB/c mice (*Mus musculus*) (n=45) with 12 weeks of age weighing (37.0±1.5 g), were supplied by the bioterium of the Fundação Oswaldo Cruz (FIOCRUZ) - Instituto Aggeu Magalhães (IAM), and kept in the experimental surgery laboratory of the Keizo Asami Immunopathology laboratory - UFPE. Each animal was kept in an individual cage, under controlled environmental conditions (12 h light/dark cycle, temperature 23±1°C and humidity of 55.0±10.0%) with free access to water and food. The animals were carefully monitored and maintained according to the ethical recommendation of the Brazilian College of Animal Experimentation (COBEA). This study was approved by the Ethics Committee on the Use of Animals (CEUA-UFPE), process N°. 23076.029229/2011-17.

The animals were divided into three groups (n=15/group) and submitted to surgical experiments under intraperitoneal anesthesia with 10.0 mg/kg of xylazine hydrochloride (2.0% w/v) and 115.0 mg/kg of ketamine hydrochloride (10.0% w/v). A standard wound (0.8 cm in diameter) was performed using surgical scissors to remove the epidermal and dermal layers of the dorsal animals skin. The treatment of each lesion was performed just once on the day of surgery by the application of the XG and XGL dressings at the wound area; the control group (C) was treated just once with 100 µL of 0.15M NaCl.

Three animals from each experimental group at 0th, 3rd, 6th, 10th, and 14th day after the surgical procedure were anesthetized and have the wound areas measured with a digital caliper. The wound area was calculated as follows: $A=\pi Rr$ (A=Wound area; R and r the main and secondary wound radii, respectively). The calculation of the degree of contraction (D) was expressed as percentage using the equations of (Ramsey, 1995), $D=100$x$(Ai-Af)/Ai$ (Ai=initial wound area; Af=wound area at the euthanasia). The results were expressed as media of three measurements±standard deviation. Then, the skin around the wound area was removed and transferred to histological cassettes and incubated in 4.0% (v/v) formaldehyde in 0.01 M PBS buffer pH 7.2, for a maximum period of 48 h. Thereafter, the formalized tissues were included in paraffin and, after microtomy, stained with Hematoxylin-Eosin (HE) and Masson's Trichrome (MT).

Blood samples (1 mL) were also collected from the anesthetized animals using the cardiac puncture technique. At the end, the animals were euthanized with lethal doses of sodium Pentobarbital (200 mg/kg) intraperitoneally. The obtained serum was used for the cytokine measurements and proteomics analysis. Milliplex cytokines immunoassay kits (Genese Produtos Diagnósticos Ltda, São Paulo, Brazil) were used for the measurements of interferon-γ (IFN-γ), tumour necrosis factor (TNF-α), interleukin 1β (IL-1β), interleukin 6 (IL-6), and interleukin 12 (IL-12). The tests were performed in triplicate according to the manufacturer's protocol. Data were collected using the MagPix Analyzer 200 flow cytometer (Luminex, Austin, USA) and the analysis was performed using Xponente software version 4.2. A four-parameter regression formula was used to calculate sample concentrations from standard curves.

2.5. Serum proteomics

Frozen serum samples from the animals of the treated groups (C, XG and XGL) were subjected to the trizol extraction method, according to the manufacturer's instructions Trizol kit (Invitroge®). The total proteins were quantified according to the instructions of the 2D Quant Kit (GE Healthcare, Piscataway, NJ, USA), using 2.0 mg/mL of bovine serum albumin (BSA) as standard. The serum proteins in the 2D gels were visualized by staining with Coomassie Brilliant Blue (CBBR250) according to Candiano et al. (2004). Gel images were acquired with a scanning resolution of 300 dpi, then analyzed with a ImageMaster 2D Platinum 7.0 software (GE Healthcare, Piscataway, NJ, USA). The quantity of each spot was normalized by the total intensity of valid spots. Serum protein spots were considered differentially expressed if the intensity changed statistically on different days.

The digestion of serum proteins in the 2D SDS-PAGE gel was performed as the method described by Shevchenko et al. (2007) with some modifications: trypsin solution (25 ng/mL) was used and the reduction and alkylation steps were omitted. The peptides were dissolved in 10 µL of 0.1 % TFA. The saturated solution (4.0 mg/mL) of alpha-cyano-4-hydroxycinnamic acid (CHCA) in 50.0% (w/v) ACN and 0.3% (w/v) TFA were mixed with an equal amount of the sample and placed on the Anchor Chip 800/384 plate (Bruker Daltonic GmbH), and left to dried in laminar air flow for recrystallization. For calibration, 0.5 µL of standard calibration peptide (Bruker Daltonik GmbH) was mixed with 0.8 µL of CHCA matrix and recrystallized as well. The samples were analyzed on a MALDI TOF/TOF mass spectrometer (Ultraflex III, Bruker Daltonics) in reflectron mode.

Mass spectra analysis was performed using the MASCOT search tool (Matrix Sciences, UK). Research was carried out using a mass tolerance set of 100 ppm and an +1-peptide loading. Trypsin was defined as a proteolytic enzyme with allowed lost cleavage. Carbamidomethylation of cysteine residues was defined as fixed modification and oxidation of methionine residues as the variable modification. MSDB, NCBInr, and Uniprot/Swissprot (release 15.2) databases were used to identify serum proteins from mice with the MASCOT server (Matrix Science, UK), available online. The identity of the serum proteins was considered significant if at least ten peptides matched those in the database, with a MASCOT peptide ion score greater than 85. The databases used were released in August 2006 for MSDB, October 2007 for NCBInr and May 2009 for UniProt/Swissprot.

2.6. Statistical analysis

All static analysis was performed using Graph Pad Prism software (version 6, 2012, USA). Student's t-test ($p<0.05$) was used in the characterization tests of the dressings. For the calculation of the area of contraction of the lesions and the analysis of the cytokine profile, was used analysis of variance ($p<0.05$), followed by the Tukey and Bonferroni tests, respectively.

3. Results and discussion

3.1. Wound dressing characterization

Infrared-ATR spectra of XG and XGL are depicted in Fig. 1. The incorporation of lectin in polysaccharide films could be attributed to O-H stretching of the polysaccharide bound to the main functional groups of the lectin (Ockman, 1981). This can be noted in the major band at approximately 3350 cm^{-1}, corresponding to the hydrogen bounds between the ConA and the xyloglucan polymeric chain. The same observation has been reported in the literature for protein incorporation into polysaccharide films (Kanmani & Rhim, 2014).

The three other important bands in XGL are located at 3240 cm^{-1} (Amide A), 1631 cm^{-1} (Amide I), and 1580 cm^{-1} (amide II). The chemical groups stretch responsible for these absorptions are the N-H, C=O, and a combination of N-H deformation and C-N stretch, respectively (Ockman, 1981). Among these three bands, the most interest is the amide I absorption, since its frequency is a measure of β-pleated sheet

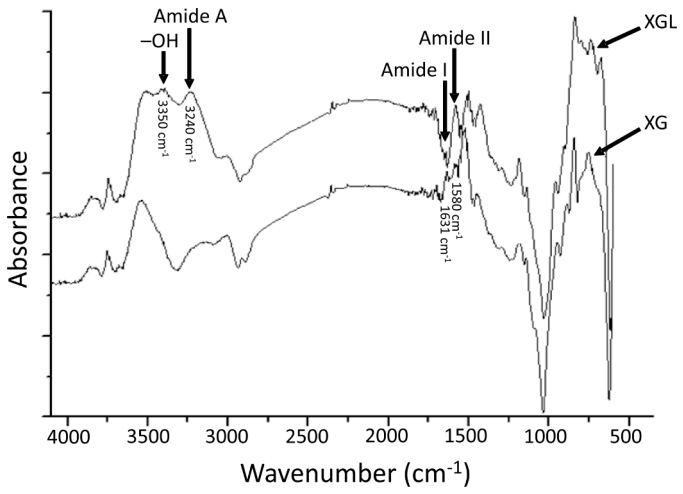

Fig. 1. Infrared-ATR spectra of xyloglucan (XG) and xyloglucan containing ConA (XGL) dressings.

conformation in the secondary structure of proteins (Kong & Yu, 2007), proving that ConA was entrapped with success inside the xyloglucan dressing.

Fluorescence microscopy images of XG and XGL-FITC are shown in Fig. 2 (A and B, respectively). XG did not show fluorescence, whereas XGL-FITC emitted fluorescence, allowing the visualization of the ConA distribution in the dressing. Jó et al. (2010) demonstrated that the critical concentration of a protein into a xyloglucan (from Tamarindus seeds) solution varies from 0.038 to 0.09 mg/mL, which is much lower than the 0.5 mg/mL used in this study. Despite this, ConA was homogeneously distributed through the microstructure of the XGL-FITC.

TEM images of the xyloglucan film labeled with ConA-Au (XGL-Au) are shown in Fig. 2 (C and D). It was possible to observe that the XG are made of micro-aggregates (small spherical bodies) with 1.0-2.0 μm. These micro-aggregations could be possible due to the xyloglucan solution characteristics of partial water-solubility (Jó et al., 2010). The individual macromolecules of xyloglucan show a balance between hydrophobic and hydrophilic centers and the substantial chain stiffness of the cellulose-like backbone facilitates intermolecular interactions, witch trend to fail in fully hydration; consequently, aggregate species remain present even in very dilute solutions (Jó et al., 2010; Picout et al., 2003). It was also possible to observe that ConA-Au of the XGL-Au was uniformly distributed inside the micro-aggregates. As noted by Zhang et al. (2013), the presence of ConA-Au was characterized by the presence of small electrodense spheres.

The humid environment prevents dehydration of the tissue, which helps in reepithelization, accelerates angiogenesis, increases the degradation of dead tissue and fibrin, and enhances the interaction of growth factors with the epithelial cells in the wound. Dressings that promote greater moisture retention are associated with less clinical infections, greater patient comfort, and reduced scarring (Kaczmarek et al., 2020; Singh, Sharma, & Dhiman, 2013). As can be seen in Table 1, XG are permeable to water vapor, with no significant changes ($p>0.05$) even with the incorporation of ConA into the matrix. The values found are like those described by Albuquerque et al. (2017) for galactomannan films ($5.60 \pm 0.39\ 10^{-7}$ g h^{-1} m^{-1} Pa^{-1}).

XG and XGL can provide adequate O_2 supply to the wound bed (Table 1), which is a prerequisite for tissue homeostasis, energy production, cell membrane maintenance, mitochondrial function, and cell repair (Singh & Pal, 2012). The incorporation of ConA in xyloglucan-based dressings did not statistically affect ($p<0.05$) these properties. Souza et al. (2015) reported similar results of oxygen

Table 1
Values of water vapor permeability (WVP), oxygen permeability (O_2P), thickness, tensile strength (TS), and elongation at break (EB) obtained from the xyloglucan (XG) and xyloglucan containing ConA (XGL) dressings.

Properties	XG	XGL
Gas barrier properties		
WVP (10^{-7}.g.h^{-1}.m^{-1}.Pa^{-1})	5.50 ± 0.21^{a}	6.02 ± 0.86^{a}
O_2P (10^{-13}.g.m.Pa^{-1}.s^{-1}.m^{-2})	6.03 ± 0.85^{a}	6.41 ± 1.40^{a}
Mechanical properties		
TS (MPa)	7.10 ± 0.42^{a}	10.28 ± 0.33^{b}
EB (%)	29.88 ± 1.32^{a}	29.37 ± 1.45^{a}
Thickness	$0.039 \pm 0,005^{b}$	0.046 ± 0.008^{a}

[ab]Different superscript letters in the same line indicate a statistically significant difference (*t* test, $p<0.05$). Data were expressed as media±standard deviation.

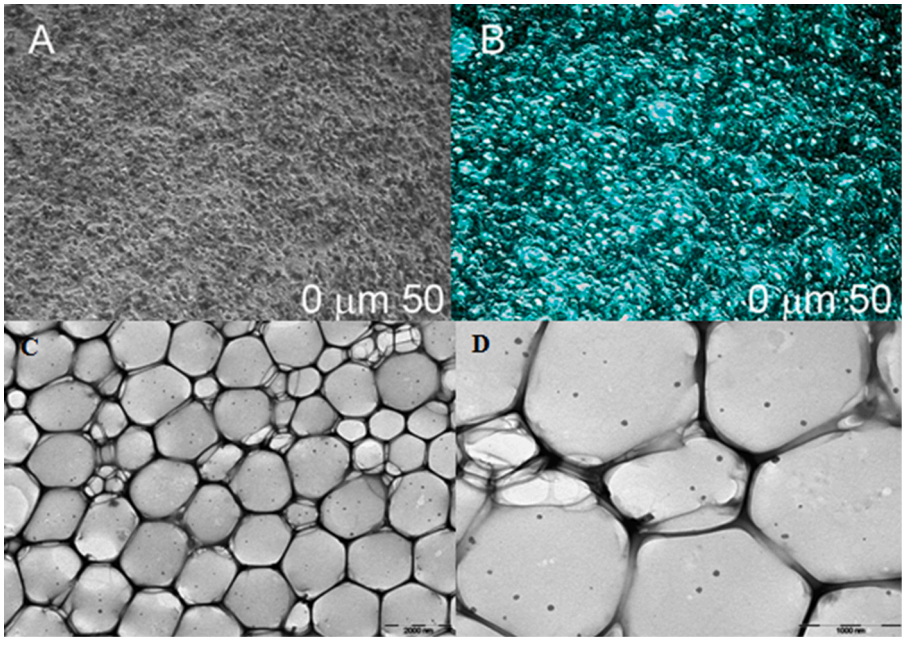

Fig. 2. Fluorescence and transmission electron microscopy images of the dressings. (A) xyloglucan dressing (XG); (B) xyloglucan dressing containing ConA-FITC (XGL-FITC); (C and D) xyloglucan dressings containing ConA-Au (XGL-Au).

permeability for chitosan-based films containing quercetin ($7.47\pm0.50.10^{-13}$.g.m.Pa^{-1}.s^{-1}.m^{-2}).

Considering the thickness of the films, it is possible to observe that increasing values of thickness generally leads to increased gas transfer resistance (Pérez-Vergara et al., 2020). As expected, the addition of conA to the filmogenic solution led to the formation of thinner films ($p>0.05$). In XGL, we can observe that even with a slight tendency to increase in WVP and O_2P (Table 1), these were not significant ($p<0.05$). We also believe that ConA led to a small increase in the available volume in the polymer matrix, thus favoring the gases penetration. Gutierrez et al. (2015), when evaluating films based on cush-cush yam and cassava starches observed a slight tendency to increase the films permeability by increasing the thickness. The barrier properties of polysaccharide based films are complex parameters that depend not only on the thickness of the films but also on the degree of polymeric crosslinking and polymer crystallinity (Siracusa, 2012).

It has been reported that ideal wound dressings must be strong enough to withstand handling and replacement, as well as elastic, to keep up with skin movements (Naseri-Nosar et al., 2017; Üstündağ Okur et al., 2019). The mechanical properties shown that the XG have low TS, however, these values were higher than the lowest acceptable value of 4 MPa for polymeric films (Rodrigues et al., 2018). Different formulations of films based on xyloglucan, extracted from *Tamarindus indica* seeds, showed TS values between 9.14–20.70 Mpa (Santos et al., 2019). The values obtained for EB are in accordance with those described in the literature for films based on xyloglucan and denote the formation of elastic films (Rodrigues et al., 2018; Santos et al., 2019). There were no differences ($p<0.05$) in EB between XG and XGL. However, the addition of ConA to the xyloglucan dressing led to the formation of stronger films, with a higher TS value, probably due to the formation of a more stable polymer matrix. These results corroborate the FTIR results where the xyloglucan chains interact with ConA through hydrogen bonds, thus leading to stronger dressings.

3.2. *In vitro assessment of ConA release, bioactive stability, and cytotoxicity of the dressings*

The ConA release rate from XGL can provide information about the

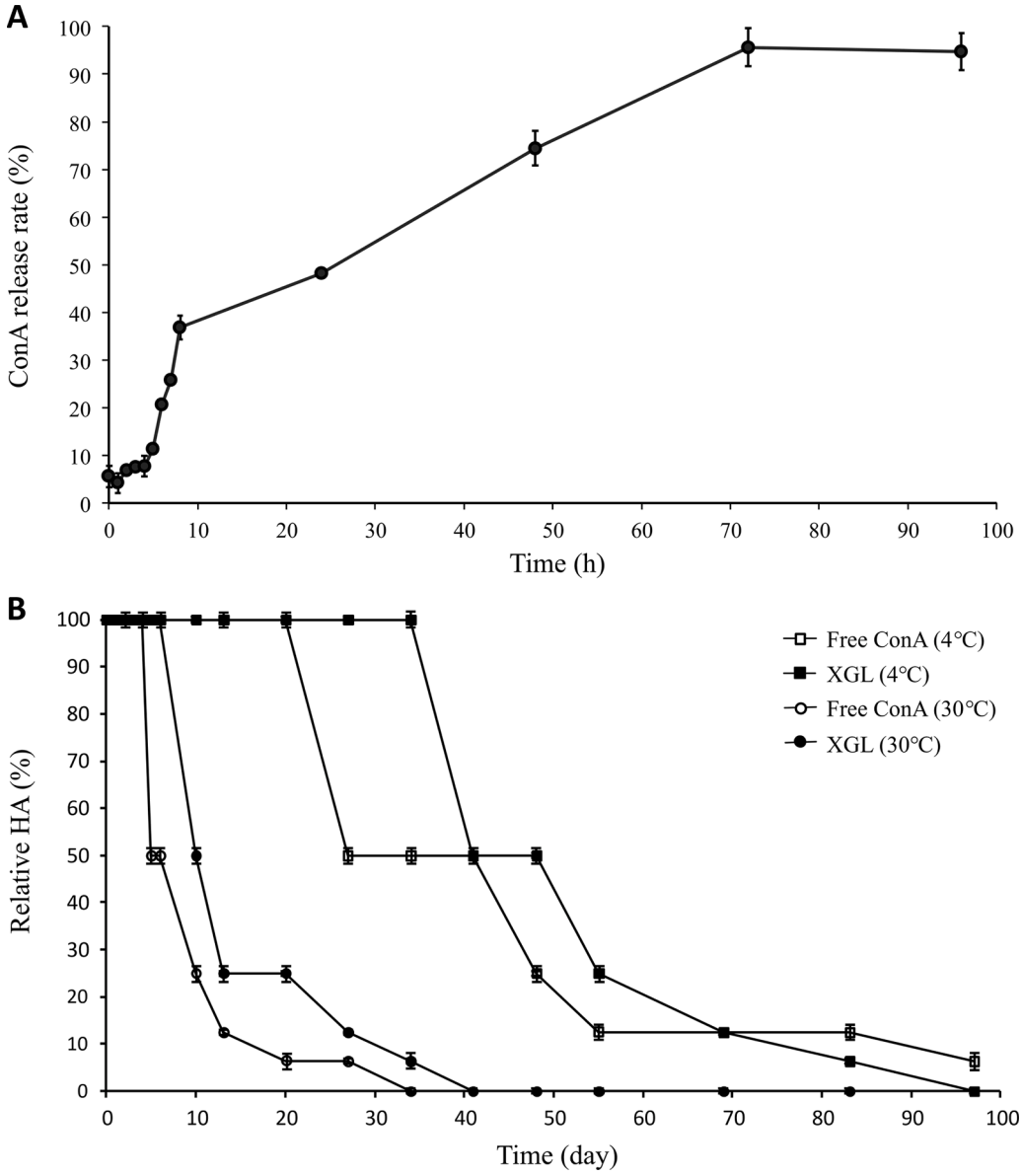

Fig. 3. ConA release rate (A), and hemagglutinating activity stability (B) from free ConA and xyloglucan dressings containing ConA (XGL) stored at 4 ° and 30°C. The results were expressed as the mean±standard deviation (n=3).

ideal time for dressing changes. In Figure 3A it is possible to observe that CoA is released from the XGL in two stages: a faster release (36.87±2.49%) in the first 8 hours followed by a slower release that reaches equilibrium within 72 h (95.67±3.92%). At the end of the process (96 h), there was an almost total dissolution of the XGL matrix in the aqueous medium and, consequently, the release of all immobilized ConA. When a solvent diffuses into a polymeric film, the mobility of the polymeric network gradually increases (matrix relaxation), allowing the entrapped macromolecules to solubilize and migrate through the swollen matrix (Üstündağ Okur et al., 2019). In addition, the lectin bioactivity was determined throughout the release test (for the first 72h), which remained stable with a HA of 1024, which did not differ from the control solution (free ConA 0.5 mg/mL).

Regarding the release kinetics, the parameter used to define the most adequate model was the evaluation of the correlation coefficient (R^2). As can be seen in table 2, the Korsmeyer and Peppas model (Korsmeyer & Peppas, 1981; Korsmeyer et al., 1983) was more adequate (R^2 of 0.98.). This model is used to assess drug release from polymeric dosage forms, where the release mechanism is not well known or when another anomalous type of release may be involved (Munday & Cox, 2000; Sujja-areevath et al.1998). The "*n*" release exponent value obtained was 0.58, thus achieving the pattern associated with an anomalous mechanism of release, non-Fickian model. Based on this result, in addition to the profile observed in the release curve (Figure 3A), we hypothesize that the ConA release occurs from the combination of three apparently independent processes: first, a small burst release (probably due to the presence of ConA in the film surface); second, due to swelling and erosion of the matrix; and finally, because to the Fick's laws.

The anomalous release process was also described for matrices based on xanthan, karaya and locust bean gum, with "*n*" values of 0.70, 0.73 and 0.77, respectively (Sujja-areevath et al.,1998). Corroborating with our results, the kinetic behavior of streptomycin release in biodegradable matrices based on xyloglucan and chitosan (1:1) also showed anomalous behavior with "*n*" of 0.89 and R^2 of 0.85 (Simi & Abraham, 2010).

The stability of ConA in the XGL in relation to free ConA, stored at 4°C and 30°C, was evaluated for 48 days measuring its hemagglutinating activity (Figure 3B). Although ConA activity has decreased significantly over storage time, the activity of immobilized ConA remained unchanged for a longer period (34 days at 4°C), suggesting that the incorporation of ConA in the xyloglucan dressings can effectively improve its stability. The increase in bioactive activity time of macromolecules after immobilization in polymeric films has also been described by Chen et al. (2020b), which developed functional wound dressings containing bromelain immobilized. In Figure 3B was also showed that the increase in storage temperature has a negative influence on the stability of ConA. While the immobilized ConA stored at 4°C maintained 100% of its activity with 10 days of storage, those that were stored at 30°C showed only 6.5% of its activity in the same period. Thus, the ideal temperature for the storage of the XGL was 4°C.

Before the *in vivo* tests, new dressings of any kind need to be tested *in vitro* to ascertain that cell viability was not affected. Concerning the cytotoxicity assay, XG showed no signal of cytotoxicity in all concentrations, whereas the XGL up to 50 μg/mL showed no cytotoxicity and the 100 μg/mL concentration was capable to maintain 88.0% of the splenocytes viable. In view of this, the CC_{50} was related to higher than 100 μg/mL concentration of the XGL. Xyloglucan extracted from tamarind was tested for cytotoxicity using intestinal epithelial cell-6 and showed non-toxicity and a cytoprotecting pattern for 125, 250, and 500 μg/mL of polysaccharide concentrations (Periasamy et al., 2018). Ajovalasit et al. (2018b) reported a moderate cytotoxicity about 75 % of viability of A549 epithelial cells for xyloglucan films (4.0 and 8.0 mg/mL).

Anterior reports shown that ConA with concentrations inferior to 0.1 mg/mL showed no cytotoxicity to hepatocytes, but concentrations superior to 0.4 mg/mL were cytotoxic (Miyagi et al., 2004). Considering that only 46% of the ConA was released from XGL in the first 24 h, which is approximately half of the toxic concentration of ConA, it is remarkable that the concentration of the lectin released from XGL is no toxic.

Table 2
Kinetics parameters of ConA release fitted four mathematical models.

Units	Zero order	First order	Higuchi	Korsmeyer-Peppas
Kinetic constants	1.04	0.02	11.00	7.34
Correlation coefficient	0.90	0.66	0.95	0.98
Release exponent	-	-	-	0.58

3.3. Wound healing analysis

The wound area retraction rate and the evolution of wound area are shown at the Figure 4. In the macroscopic findings, a significant difference ($p<0.05$) was observed in terms of the contraction of the lesion after the sixth day, where the XGL group presented an area of 0.08±0.01 cm^2 and the groups C and XG still had areas of 0.21±0.03 cm^2.

On the tenth day for the XGL group, the wound has already completely closed, while the C and XG groups still had an area of 0.03±0.01 cm^2. Sheets containing 3.0% (w/v) of xyloglucan applied in deep skin wounds showed similar results to the XG and XGL of this work reducing the wound area for about 40.0% (Hirose et al., 2019). Histological evaluation of the healing process of wounds in groups C, XG, and XGL was accompanied by the presence of crust, infiltration of inflammatory cells, angiogenesis, collagen impregnation, formation of granulation tissue, and re-epithelialization of the lesion (Figure 5).

On the third day after surgery, group C showed the presence of a crust consisting of plasma and cellular debris occupying the most superficial region of the lesion, with the presence of a mild inflammatory infiltrate. On the other hand, the XG group presented in addition to the crust and intense inflammatory infiltrate, a clear angiogenesis. The XGL group, in addition to the elements already mentioned for the other groups, also observed the presence of fibroblasts. These data indicate that both groups XG and XGL already showed signs of advanced healing with three days of treatment when compared to group C. The presence of inflammatory cell, mainly macrophage, is fundamental to the healing process allowing the degradation and elimination of damaged components from extracellular matrix (ECM) in epithelial tissue, such as collagen and elastin (Singer & Clark, 1999).

On the sixth day, it was still possible to observe the presence of inflammatory cells and a dense crust. However, the XG group has already started to present fibrovascular granulation tissue and a thinner crust. As for the XGL group, in addition to fibrovascular granulation tissue, it was possible to observe an intense collagen deposition and vascular neoformation, indicating that this group with six days of treatment was already in the proliferative phase of the healing process (Singer & Clark, 1999; Tottoli et al., 2020). During this phase, metalloproteinases (MMP) are the main components of the ECM responsible for the proteolytic remodeling process of damage tissues (Gearing et al., 1994). These enzymes can be produced by several types of skin cells, such as fibroblasts, endothelial cells, mast cells and polymorphonuclear cells, having an important role in various physiological situations, including: morphogenesis, tissue development, tissue repair and angiogenesis (Kähäri & Saarialho-Kere, 1997). Previous works, reported that ConA can induce the production of MMP-9 by lymphocytes, witch in association with other MMP from ECM can improve the healing process (Dubois et al., 1998; Silva et al., 2009).

On the tenth day, it was possible to observe the maturation of granulation tissue and the beginning of collagen deposition for groups C and XG, however the XGL group already shown a reduction in collagen deposition, thus characterizing the beginning of the remodeling and reepithelization phase of the injury. On the fourteenth day, collagen

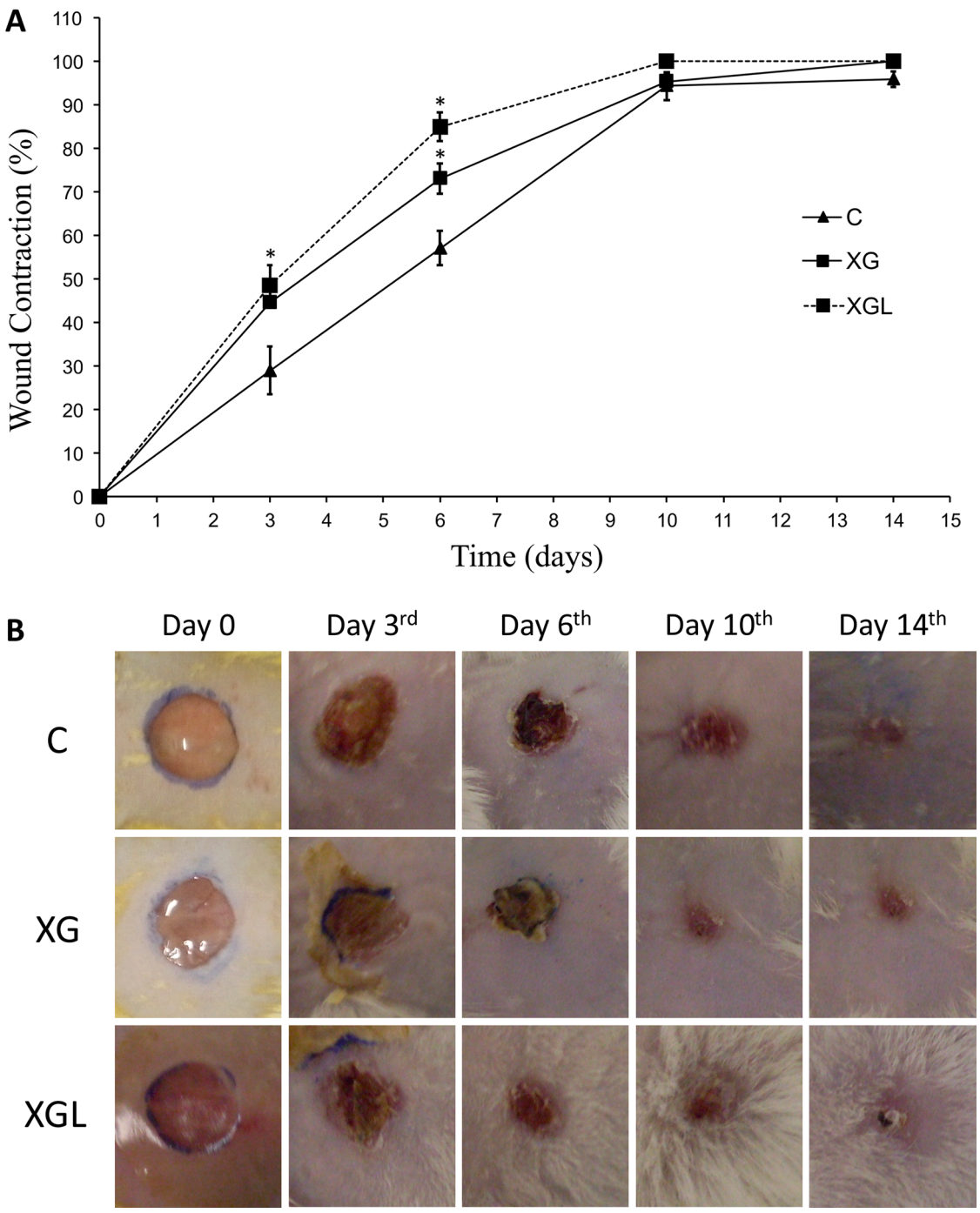

Fig. 4. Wound contraction rate of the macroscopic measurements (A) and the wound imaging of circular excision wound areas at 0, 3rd, 6th, 10th and 14th days (B). C: control (saline); XG: xyloglucan dressing; XGL: xyloglucan dressing containing ConA. The wound area was expressed by the means±standard deviation (n=3) and the statistic analysis performed by ANOVA followed by the Tukey test (*p<0.05).

deposition in group C was still visible, but groups XG and XGL already had a well-organized ECM with the presence of newly formed vessels, dermal attachments and well-stratified epithelial tissue. Xyloglucan membranes with and without Cramoll lectin, after 12 days, in a daily treatment of cutaneous wounds of diabetic mice, could accelerate the wound reepithelization with typical characteristics of healthy skin (Andrade et al., 2021). Although the wounds were performed in health mice, our work showed similar results despite a unique application of the dressings XG and XGL.

3.4.1. *Cytokines profile*

The cytokines profile identified in the serum of animals treated with XG and XGL, in addition to control group, are presented in Figure 6. During the *in vivo* wound healing experiment, the immunomodulation of the cytokines mobilized during the treatments were evaluated in terms of the inflammation response by the production of pro-inflammatory cytokines like interferon-γ (IFN-γ), tumour necrosis factor (TNF-α), interleukin 1β (IL-1β), interleukin 6 (IL-6), and interleukin 12 (IL-12).

IFN-γ is a major cytokine that plays a key role in innate and adaptive immune responses (Biringanine et al., 2005). Regarding the results for IFN-γ, it was possible to observe that XG and XGL significantly reduced

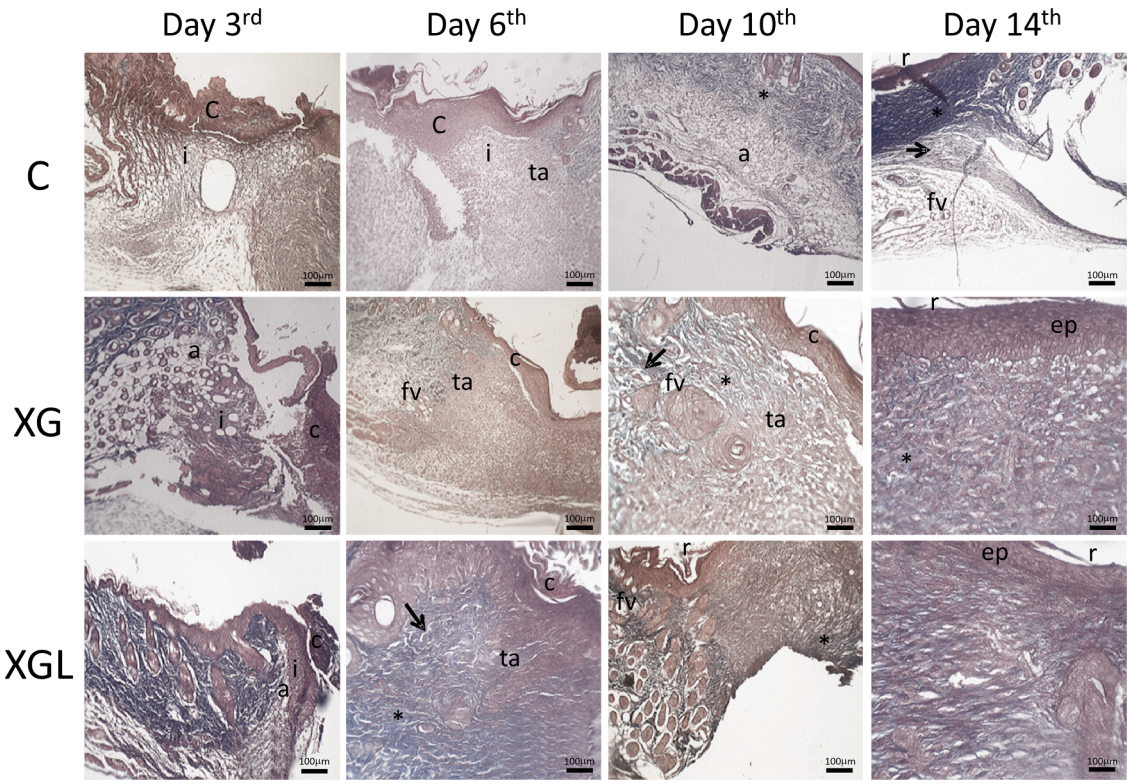

Fig. 5. Histologic photomicrograph of skin wounds of mice from control (C), xyloglucan dressing (XG) and xyloglucan dressing containing ConA (XGL) groups at 3rd, 6th, 10th and 14th of treatment, stained with Masson's trichrome. Scale bar: 100 µm. Legend: c: crust; i: inflammatory infiltrate; ta: transition area; a: angiogenesis; r: re-epithelialization; fv: fibrovascular granulation tissue; ep: stratified epidermis; arrow: fibroblasts; asterisk: collagen fibers.

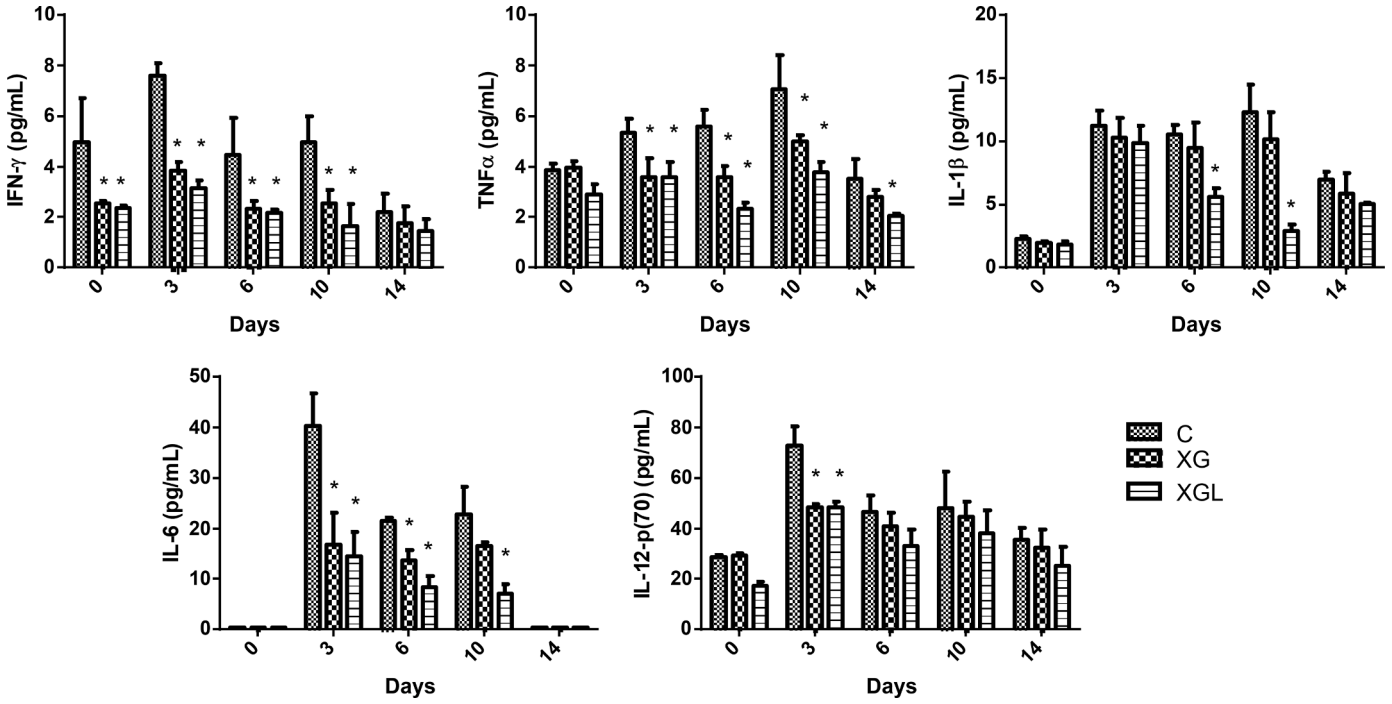

Fig. 6. Cytokine profile of the wound healing process at the day of the surgery and after 3rd, 6th, 10th and 14th day. C: control (saline); XG: xyloglucan dressing; XGL: xyloglucan dressing containing ConA. The results were expressed as the mean±standard deviation (n=3) and the statistic analysis performed by ANOVA followed by the Bonferroni test (*$p<0.05$).

the production of interferon from 0th to 10th day when compared to the negative control group; in addition, no difference was observed between the XG and XGL treatments for the entire experimental range. The same pattern of significant decrease in cytokine secretion was observed for TNF-α on specific days. TNF-α is a cytokine produced by monocytes/macrophages in a cellular concentration-dependent manner. It is

effective in regulating inflammation and autoimmunity, especially due to the ability to activate NK cells. Our results demonstrate that XGL decreased TNF-α secretion when compared to the control group from the 3rd day and it was also possible to observe statistical differences between XG and XGL treated groups at 0th, 6th, 10th, and 14th days. In this case, the immunomodulatory activity of ConA from the XGL films is congruent with what has been reported for mannose binding lectins, i.e., the lectins' capability to reduce the pro-inflammatory cytokine production, mainly TNF-α and IL-10 (Silva et al., 2016).

Interleukins, like IL-1β, IL-6, and IL-12, are pro-inflammatory cytokines generated by a variety of immune cells, which regulate the cellular interaction between leucocytes and other cells. They are involved in maintaining body homeostasis against infections (Huang et al., 2019). The IL-1β secretion was significantly decreased by XGL treatment from 6th to 10th days in comparison with both XG and the control groups. The serum level of IL-6 was detected only between the 3rd and 10th day, especially when the inflammatory and remodelling phase of the healing process is on the peak (Tottoli et al., 2020). In this period, XG and XGL treatments were different from the control group, proving its anti-inflammatory activities and corroborating the histologic analysis. Only in the remodelling phase (from the 6th to 10th days) that the levels of IL-6 showed difference between the XG and XGL treatments. In the peak of the inflammatory phase (3rd day), it was also observed a significant reduction in the serum level of IL-12 for the animals treated with the XG and XGL films. These results urging that the XDL possess a good anti-inflammatory activity during the healing process, especially in the early phase, which is a top priority characteristic in the field of dressings.

From the 6th, no significant difference was observed on the serum level of IL-12 among the treated groups. During the inflammatory phase of the wound healing, occurs a M2 macrophage subset formation, which regulate inflammation by expressing cytokines as IL-1, IL-10, and IL-12, as well as several growth factors to promote fibroblast proliferation, extracellular matrix synthesis, and angiogenesis (Kotwal & Chien, 2017; Serra et al., 2017; Xiao et al., 2020). The non-reduction of IL-12 on the treated groups after the 6th day suggests that these M2 macrophage are contributing actively with the remodelling and reepithelization phase of the wound.

3.4.2. Serum proteome

Proteome profile on the 3rd day after surgery was performed to identify the serum proteins that were differentially expressed from the XGL group to the XG and control groups and that possessed a reported influence in stimulating the wound healing process. Seven expressed proteins were identified and characterized by proteomics analysis (Table 3) from the 2D gel electrophoretogram of the serum proteins (Supplementary material). The proteins that showed an increase expression were α1-antitrypsin, serine peptidase inhibitor, vitamin D-binding protein and hemopexin, while apolipoprotein A1, albumin and transferrin showed a decrease expression. These proteins are closely linked to the inflammatory phase of the healing process, playing several roles to delay the inflammation and pain and the tissue damage caused by the injury.

It is known that, during inflammatory processes, HDL can undergo modifications and become pro-inflammatory (Ansell et al., 2007). Apolipoprotein A1 (spot 1) is the main component of HDL under normal conditions. However, during inflammatory events, its production can be suppressed by cytokines, and the apolipoprotein A1 containing lipids are rapidly catabolized, thus, promoting an anti-inflammatory response (Georgila, Vyrla, & Drakos, 2019). The decreased expression of apolipoprotein A1 in animals treated with XGL during the inflammatory phase of the wound, could be related to this phenomenon, which is beneficial to the healing process.

During the inflammatory phase of the wound, the XGL treatment was not capable in maintain the serum levels of albumin (spot 2), and its decreased expression in comparison with the XG and control groups corroborates with a greater local protein catabolism that could be being stimulated by the XGL. The local proteolysis is an important debridement event that occur during the inflammatory phase of the wound (Tottoli et al., 2020) and the devitalized tissue removal is a fundamental process for tissue repair (Lumbers, 2018).

The α1-antitrypsin (spot 3), together with serine peptidase inhibitor, clade A (spot 4), had their expression increased during the inflammatory phase of the wound healing in the animals treated with XGL. The expression of serpins during inflammatory phase can increase the collagen type I production, accelerating the healing process and limiting the tissue damage caused by the wound (Congote et al., 2008; Lucas et al., 2018). The vitamin D binding protein (spot 5) is a circulating multifunctional plasma protein that can significantly enhance the chemotactic activity of neutrophil, modulating the immune system (Kew, 2019). Besides that, it plays an additional role in preventing the polymerization of actin, helping the body in the healing of damaged tissues (Meier et al., 2006). During the inflammatory phase of the wound healing, large quantities of actin from the tissue injury can be released into extracellular fluids where the protein escapes from normal intracellular scavenger mechanisms and spontaneously form F-actin filaments. Higher concentrations of F-actin filaments in plasma can induce microcirculatory diseases and to prevent the its accumulation, the vitamin D binding protein decrease the plasma concentration of free actin (Haddad et al., 1990; Meier et al., 2006). The treatment with the XGL increased the vitamin D binding protein expression during the inflammatory phase of the healing process proving its beneficial efficacy in the wound care.

Hemopexin is a heme plasma glycoprotein which, after haptoglobin, acting as a second line of barrier against heme's pro-inflammatory and pro-oxidant effects and increase its detoxification (Chen et al., 2020a; Kanno et al., 2017). The expression of hemopexin (spot 6) was up-regulated during the inflammatory phase (Table 3). These indicate that the XGL could be involved in an earlier anti-inflammatory response and the suppression of oxidative stress to accelerate the wound healing. Equally to serum albumin, transferrin (spot 7) is a negative acute phase protein, which expression decreased in the animals treated with the XGL. Transferrin is an iron-binding glycoprotein that control the level of free iron in biological fluids. Decrease plasma levels of transferrin lead to the iron excess in the extracellular matrix, which has a deleterious effect on tissue repair (Crichton & Charloteaux-Wauters, 1987; Recalcati et al., 2019). To preventing this, activated M1-macrophages, during the inflammatory phase of the wound healing, plays an important role in the

Table 3
Mass spectrometric features of distinguished serum protein identified during the healing process of the animals treated with the xyloglucan dressing containing ConA (XGL) in comparison to the xyloglucan dressing (XG) and control (saline) groups on 3rd day after surgery.

Spot	Identity	Score	TheoreticalIsoelectricPoint	MolecularWeight(kDa)	Relative expression
1	Apolipoprotein A1 precursor	165	5.52	30.3	decrease
2	Serum albumin precursor	107	5.75	70.7	decrease
3	α-1 antitrypsin (SERPIN-1) precursor	90	5.33	46.0	increase
4	Serine (or cysteine) peptidase inhibitor clade A, member 3K	138	5.05	46.9	increase
5	Vitamin D-binding protein	101	5.26	54.6	increase
6	Hemopexin precursor	88	7.92	52.0	increase
7	Serotransferrin precursor	106	6.94	78.8	decrease

iron metabolism (Recalcati, Locati, & Cairo, 2012). Iron sequestration by M1-macrophages is an efficient bacteriostatic effect in host defense (Ganz & Nemeth, 2015). Considering this, the modulation of important proteins expression in the tissue injury of the animals treated with XGL compared with the XG and control groups, could be explained by a non-contaminated, anti-inflammatory and accelerated healing promotion.

4. Conclusion

This work mainly addressed the relationships between physico-chemical and morphological properties of a xyloglucan wound dressing, its capacity as biomolecule carrier and *in vivo* wound healing application. The ConA incorporated in the xyloglucan dressing maintained its biological activity for fourteen days in a controlled-release manner. XG and XGL were non-toxic, homogeneous, easy to handle, and flexible, suggesting that it can provide a safe protection to the wound during healing. Although the XGL showed a better wound contraction compared with the XG, both were capable of accelerate the wound healing, promoting less infiltration of inflammatory cells, more angiogenesis, remodeling, and early epithelization. Further, both films alleviate the inflammation phase by reducing the production of pro-inflammatory cytokines, like IL-1β, IL-6, IL-12, INF-γ, and TNF-α. The XGL also showed a good healing activity in promote the up- and down-regulation of important proteins associated in the wound repair. Finally, all these findings suggest that both XG and XGL may represent a good therapeutic approach for advanced wound healing applications.

Declaration of Competing Interest

The authors report no declarations of interest.

Acknowledgements

The authors are grateful for the financial support for research grants from the Conselho Nacional de Desenvolvimento Científico e Tecnológico (CNPq), Coordenação de Aperfeiçoamento de Pessoal de Nível Superior (CAPES) and the Fundação de Amparo à Ciência e Tecnologia do Estado de Pernambuco (FACEPE). We are grateful to the Centro de Tecnologias Estratégicas do Nordeste (CETENE) and to the Laboratório de Imunopatologia Keizo Asami-LIKA at the Universidade Federal de Pernambuco (UFPE) for access to its installation and technical assistance.

CRediT authorship contribution statement

I.R.S.A: Methodology, validation, formal analysis, investigation, data curation, original draft writing, M.P.S.: Methodology, formal analysis, investigation, data curation, writing, review and editing, P.A.G.S.: formal analysis, investigation, data curation, writing, review and editing, P.B.S. Albuquerque: formal analysis, investigation, data curation, writing, review and editing, T.D. Silva: formal analysis, investigation, data curation, P.L.M.: formal analysis, investigation, data curation, M.V. S.: research supervision, resources, M.T.S.C.: research supervision, resources, A.A.V.: research supervision, resources, M.G.C.-da-C.: research supervision, resources, project administration.

Supplementary materials

Supplementary material associated with this article can be found, in the online version, at doi:10.1016/j.carpta.2021.100136.

References

Ajith, G., Goyal, A. S., Rodrigues, F. C., & Thakur, G. (2021). Natural polysaccharides for wound healing. *Food, Medical, and Environmental Applications of Polysaccharides* (pp. 341–379). Elsevier Ltd. https://doi.org/10.1016/B978-0-12-819239-9.00019-1.

Ajovalasit, A., Caccami, M. C., Amendola, S., Sabatino, M. A., Alotta, G., Zingales, M., Giacomazza, D., Dispenza, C., Marrocco, G., & Dispenza, C. (2018b). Development and characterization of xyloglucan-poly(vinyl alcohol) hydrogel membrane for Wireless Smart wound dressings. *European Polymer Journal, 106*(June), 214–222. https://doi.org/10.1016/j.eurpolymj.2018.07.038.

Ajovalasit, A., Sabatino, M. A., Todaro, S., Alessi, S., Giacomazza, D., Picone, P., Di Carlo, M., & Dispenza, C. (2018a). Xyloglucan-based hydrogel films for wound dressing: Structure-property relationships. *Carbohydrate Polymers, 179*(July 2017), 262–272. https://doi.org/10.1016/j.carbpol.2017.09.092.

Albuquerque, P. B. S., Soares, P. A. G., Aragão-Neto, A. C., Albuquerque, G. S., Silva, L. C. N., Lima-Ribeiro, M. H. M., Neto, Silva, J., C., Coelho, L. C. B. B., Correia, M. T. S., Teixeira, J. A. C., & Carneiro-da-Cunha, M. G. (2017). Healing activity evaluation of the galactomannan film obtained from Cassia grandis seeds with immobilized Cratylia mollis seed lectin. *International Journal of Biological Macromolecules, 102*, 749–757. https://doi.org/10.1016/j.ijbiomac.2017.04.064.

Andrade, F. M., Neves, F. P. A., Albuquerque, P. B. S., Aragão-neto, A. C., Jandú, J. J. B., Coelho, L. C. B. B., Lima-Ribeiro, M. H. M., Teixeira, A. A. C., Carneiro-da-Cunha, M. G., Teixeira, V. W., & Correia, M. T. S. (2021). Healing activities of Cramoll and xyloglucan membrane in cutaneous wounds of diabetic mice. *Journal of Immunology and Regenerative Medicine, 13*, Article 100045. https://doi.org/10.1016/j.regen.2021.100045.

Ansell, B. J., Fonarow, G. C., Navab, M., & Fogelman, A. M. (2007). Modifying the anti-inflammatory effects of high-density lipoprotein. *Current Atherosclerosis Reports, 9*(1), 57–63. https://doi.org/10.1007/BF02693941.

Arruda, I. R. S., Albuquerque, P. B. S., Santos, G. R. C., Silva, A. G., Mourão, P. A. S., Correia, M. T. S., Vicente, A. A., & Carneiro-da-Cunha, M. G. (2015). Structure and rheological properties of a xyloglucan extracted from Hymenaea courbaril var. courbaril seeds. *International Journal of Biological Macromolecules, 73*, 31–38. https://doi.org/10.1016/j.ijbiomac.2014.11.001.

ASTM. (2010). ASTM D882-10: Standard test methods for tensile properties of thin plastic sheeting, method D882-10. Philadelphia, PA: American Society for Testing and Materials. *ASTM Annual Book of Standards, 87*, 3–5. https://www.astm.org/Standards/D882.htm.

ASTM. (2017). ASTM D3985 - 17: Standard Test Method for Oxygen Gas Transmission Rate Through Plastic Film and Sheeting Using a Coulometric Sensor. *ASTM Annual Book of Standards, 7*. https://www.astm.org/Standards/D3985.htm.

Bemer, V., & Truffa-Bachi, P. (1996). T cell activation by concanavalin A in the presence of cyclosporin A: Immunosuppressor withdrawal induces NFATp translocation and interleukin-2 gene transcription. *European Journal of Immunology, 26*(7), 1481–1488. https://doi.org/10.1002/eji.1830260712.

Biringanine, G., Vray, B., Vercruysse, V., Vanhaelen-Fastré, R., Vanhaelen, M., & Duez, P. (2005). Polysaccharides extracted from the leaves of Plantago palmata Hook.f. induce nitric oxide and tumor necrosis factor-α production by interferon-γ-activated macrophages. *Nitric Oxide - Biology and Chemistry, 12*(1), 1–8. https://doi.org/10.1016/j.niox.2004.10.008.

Bradford, M. M. (1976). A rapid and sensitive method for the quantitation of microgram quantities of protein utilizing the principle of protein-dye binding. *Analytical Biochemistry, 72*(1–2), 248–254. https://doi.org/10.1016/0003-2697(76)90527-3.

Candiano, G., Bruschi, M., Musante, L., Santucci, L., Ghiggeri, G. M., Carnemolla, B., Orecchia, P., Zardi, L., & Righetti, P. G. (2004). Blue silver: A very sensitive colloidal Coomassie G-250 staining for proteome analysis. *Electrophoresis, 25*(9), 1327–1333. https://doi.org/10.1002/elps.200305844.

Chen, R. F., Yang, M. Y., Wang, C. J., Wang, C. T., & Kuo, Y. R. (2020a). Proteomic analysis of peri-wounding tissue expressions in extracorporeal shock wave enhanced diabetic wound healing in a streptozotocin-induced diabetes model. *International Journal of Molecular Sciences, 21*(15), 1–13. https://doi.org/10.3390/ijms21155445.

Chen, X., Wang, X., Wang, S., Zhang, X., Yu, J., & Wang, C. (2020b). Mussel-inspired polydopamine-assisted bromelain immobilization onto electrospun fibrous membrane for potential application as wound dressing. *Materials Science and Engineering C, 110*(December 2019), Article 110624. https://doi.org/10.1016/j.msec.2019.110624.

Coelho, L. C. B. B., Silva, P. M. D. S., Lima, V. L. D. M., Pontual, E. V., Paiva, P. M. G., Napoleão, T. H., & Correia, M. T. D. S. (2017). Lectins, Interconnecting Proteins with Biotechnological/Pharmacological and Therapeutic Applications. *Evidence-Based Complementary and Alternative Medicine, 2017*. https://doi.org/10.1155/2017/1594074.

Congote, L. F., Temmel, N., Sadvakassova, G., & Dobocan, M. C. (2008). Comparison of the effects of serpin A1, a recombinant serpin A1-IGF chimera and serpin A1 C-terminal peptide on wound healing. *Peptides, 29*(1), 39–46. https://doi.org/10.1016/j.peptides.2007.10.011.

Correia, M. T. S., & Coelho, L. C. B. B. (1995). Purification of a glucose/mannose specific lectin, isoform 1, from seeds of Cratylia mollis mart. (Camaratu Bean). *Applied Biochemistry and Biotechnology, 55*(3), 261–273. https://doi.org/10.1007/BF02786865.

CRICHTON, R. R., & CHARLOTEAUX-WAUTERS, M. (1987). Iron transport and storage. *European Journal of Biochemistry, 164*(3), 485–506. https://doi.org/10.1111/j.1432-1033.1987.tb11155.x.

Dubois, B., Peumans, W. J., Van Damme, E. J. M., Van Damme, J., & Opdenakker, G. (1998). Regulation of gelatinase B (MMP-9) in leukocytes by plant lectins. *FEBS Letters, 427*(2), 275–278. https://doi.org/10.1016/S0014-5793(98)00449-9.

Dwyer, J. M., & Johnson, C. (1981). The use of concanavalin A to study the immunoregulation of human T cells. *Clinical and Experimental Immunology, 46*(2), 237–249. http://www.ncbi.nlm.nih.gov/pubmed/6461456%0Ahttp://www.pubmedcentral.nih.gov/articlerender.fcgi?artid=PMC1536405.

Farias, M. D. P., Albuquerque, P. B. S., Soares, P. A. G., de Sá, D. M. A. T., Vicente, A. A., & Carneiro-da-Cunha, M. G. (2018). Xyloglucan from Hymenaea courbaril var. courbaril seeds as encapsulating agent of L-ascorbic acid. *International Journal of Biological Macromolecules, 107*, 1559–1566. https://doi.org/10.1016/j.ijbiomac.2017.10.016.

Ganz, T., & Nemeth, E. (2015). Iron homeostasis in host defence and inflammation. *Nature Reviews Immunology, 15*(8), 500–510. https://doi.org/10.1038/nri3863.

Gearing, A. J. H., Beckett, P., Christodoulou, M., Churchill, M., Clements, J., Davidson, A. H., , … Gordon, J. L., et al. (1994). Processing of tumor necrosis factor-a precursor by metalloproteinases. *Nature, 370*(6490), 555–557. https://doi.org/10.1038/370555a0.

Georgila, K., Vyrla, D., & Drakos, E. (2019). *Apolipoprotein A-I (ApoA-I), Immunity, Inflammation and Cancer, 4*, 1–25.

Gutiérrez, T. J., Tapia, M. S., Pérez, E., & Famá, L. (2015). Structural and mechanical properties of edible films made from native and modified cush-cush yam and cassava starch. *Food Hydrocolloids, 45*, 211–217. https://doi.org/10.1016/j.foodhyd.2014.11.017.

Haddad, J. G., Harper, K. D., Guoth, M., Pietra, G. G., & Sanger, J. W. (1990). Angiopathic consequences of saturating the plasma scavenger system for actin. *Proceedings of the National Academy of Sciences of the United States of America, 87*(4), 1381–1385. https://doi.org/10.1073/pnas.87.4.1381.

Hayashi, T., & Kaida, R. (2011). Functions of xyloglucan in plant cells. *Molecular Plant, 4*(1), 17–24. https://doi.org/10.1093/mp/ssq063.

Hirose, K., Sasatsu, M., Toraishi, T., & Onishi, H. (2019). Novel xyloglucan sheet for the treatment of deep wounds: Preparation, physicochemical characteristics, and in vivo healing effects. *Biological and Pharmaceutical Bulletin, 42*(8), 1409–1414. https://doi.org/10.1248/bpb.b18-00764.

Huang, L., Shen, M., Morris, G. A., & Xie, J. (2019). Sulfated polysaccharides: Immunomodulation and signaling mechanisms. *Trends in Food Science and Technology, 92*(235), 1–11. https://doi.org/10.1016/j.tifs.2019.08.008.

Jó, T. A., Petri, D. F. S., Beltramini, L. M., Lucyszyn, N., & Sierakowski, M. R. (2010). Xyloglucan nano-aggregates: Physico-chemical characterisation in buffer solution and potential application as a carrier for camptothecin, an anti-cancer drug. *Carbohydrate Polymers, 82*(2), 355–362. https://doi.org/10.1016/j.carbpol.2010.04.072.

Kaczmarek, B., Mazur, O., Miłek, O., Michalska-Sionkowska, M., Osyczka, A. M., & Kleszczyński, K. (2020). Development of tannic acid-enriched materials modified by poly(ethylene glycol) for potential applications as wound dressing. *Progress in Biomaterials, 9*(3), 115–123. https://doi.org/10.1007/s40204-020-00136-1.

Kähäri, V. M., & Saarialho-Kere, U. (1997). Matrix metalloproteinases in skin. *Experimental Dermatology, 6*(5), 199–213. https://doi.org/10.1111/j.1600-0625.1997.tb00164.x.

Kanmani, P., & Rhim, J. W. (2014). Antimicrobial and physical-mechanical properties of agar-based films incorporated with grapefruit seed extract. *Carbohydrate Polymers, 102*(1), 708–716. https://doi.org/10.1016/j.carbpol.2013.10.099.

Kanno, T., Yasutake, K., Tanaka, K., Hadano, S., & Ikeda, J. E. (2017). A novel function of N-linked glycoproteins, alpha-2-HS-glycoprotein and hemopexin: Implications for small molecule compound-mediated neuroprotection. *PLoS ONE, 12*(10), 1–21. https://doi.org/10.1371/journal.pone.0186227.

Kew, R. R. (2019). The Vitamin D binding protein and inflammatory injury: A mediator or sentinel of tissue damage? *Frontiers in Endocrinology, 10*(JULY), 1–10. https://doi.org/10.3389/fendo.2019.00470.

Kong, J., & Yu, S. (2007). Fourier transform infrared spectroscopic analysis of protein secondary structures. *Acta Biochimica et Biophysica Sinica, 39*(8), 549–559. https://doi.org/10.1111/j.1745-7270.2007.00320.x.

Kordestani, S. S. (2019). Wound Healing Process. *Atlas of Wound Healing*, 11–22. https://doi.org/10.1016/b978-0-323-67968-8.00003-3. https://doi.

Korsmeyer, R. W., Gurny, R., Doelker, E. M., Buri, P., & Peppas, N. A. (1983). Mechanism of solute release from porous hydrophilic polymers. *International Journal of Pharmaceutics, 15*, 25–35.

Korsmeyer, R. W., & Peppas, N. A. (1981). Macromolecular and modeling aspects of swelling controlled systems. In T. J. Roseman, & S. Z. Mansdorf (Eds.), *Controlled release delivery systems* (pp. 77–90). New York: Marcel Dekker.

Kotwal, J. G., & Chien, S. (2017). Evolutionary Aspects of Macrophages. *Macrophages Origin, Functions and Biointervention, 62*, 3–22. https://doi.org/10.1007/978-3-319-54090-0.

Kulkarni, A. D., Joshi, A. A., Patil, C. L., Amale, P. D., Patel, H. M., Surana, S. J., Belgamwar, V. S., Chaudhari, K. S., & Pardeshi, C. V. (2017). Xyloglucan: A functional biomacromolecule for drug delivery applications. *International Journal of Biological Macromolecules, 104*, 799–812. https://doi.org/10.1016/j.ijbiomac.2017.06.088.

Liu, W., Du, H., Zhang, M., Liu, K., Liu, H., Xie, H., Zhang, X., & Si, C. (2020). Bacterial Cellulose-Based Composite Scaffolds for Biomedical Applications: A Review. *ACS Sustainable Chemistry & Engineering, 8*(20), 7536–7562. https://doi.org/10.1021/acssuschemeng.0c00125. https://dx.doi.org/.

Lucas, A., Yaron, J. R., Zhang, L., Macaulay, C., & McFadden, G. (2018). Serpins: Development for therapeutic applications. *Methods in Molecular Biology, 1826*, 255–265. https://doi.org/10.1007/978-1-4939-8645-3_17.

Lumbers, M. (2018). Wound debridement: Choices and practice. *British Journal of Nursing, 27*(15), S16–S20. https://doi.org/10.12968/bjon.2018.27.15.S16.

Meier, U., Gressner, O., Lammert, F., & Gressner, A. M. (2006). Gc-globulin: Roles in response to injury. *Clinical Chemistry, 52*(7), 1247–1253. https://doi.org/10.1373/clinchem.2005.065680.

Miyagi, T., Takehara, T., Tatsumi, T., Suzuki, T., Jinushi, M., Kanazawa, Y., Hiramatsu, N., Kanto, T., Tsuji, S., Hori, M., & Hayashi, N. (2004). Concanavalin A injection activates intrahepatic innate immune cells to provoke an antitumor effect in murine liver. *Hepatology, 40*(5), 1190–1196. https://doi.org/10.1002/hep.20447.

Munday, D. L., & Cox, P. J. (2000). Compressed xanthan and karaya gum matrices: hydration, erosion and drug release mechanisms. *International Journal of Pharmaceutics, 203*, 179–192. https://doi.org/10.1016/S0378-5173(00)00444-0.

Naseri-Nosar, M., Farzamfar, S., Sahrapeyma, H., Ghorbani, S., Bastami, F., Vaez, A., & Salehi, M. (2017). Cerium oxide nanoparticle-containing poly (ε-caprolactone)/gelatin electrospun film as a potential wound dressing material: In vitro and in vivo evaluation. *Materials Science and Engineering C, 81*(July), 366–372. https://doi.org/10.1016/j.msec.2017.08.013.

Nishinari, K., Takemasa, M., Suzuki, Y., & Yamatoya, K. (2021). Xyloglucan. *Woodhead Publishing Series in Food Science, Technology and Nutrition, Handbook of Hydrocolloids* (3rd Edition, pp. 317–365). Woodhead Publishing. https://doi.org/10.1016/B978-0-12-820104-6.00029-2.

Ockman, N. (1981). Interaction of monolayers of concanavalin A with mono- and polysaccharides A study by means of infrared-attenuated total reflectance spectroscopy. *BBA - Biomembranes, 643*(1), 220–232. https://doi.org/10.1016/0005-2736(81)90235-2.

Pardeshi, C. V., Kulkarni, A. D., Belgamwar, V. S., & Surana, S. J. (2018). Xyloglucan for drug delivery applications. *Fundamental Biomaterials: Polymers*. Elsevier Ltd.. https://doi.org/10.1016/B978-0-08-102194-1.00007-4

Pereira, E. M. A., Sierakowski, M. R., Jó, T. A., Moreira, R. A., Monteiro-Moreira, A. C. O., França, R. F. O., Fonseca, B. A. L., & Petri, D. F. S. (2008). Lectins and/or xyloglucans/alginate layers as supports for immobilization of dengue virus particles. *Colloids and Surfaces B: Biointerfaces, 66*(1), 45–52. https://doi.org/10.1016/j.colsurfb.2008.05.013.

Pereira, V. R. A., Lorena, V. M. B., Silva, Galvao Da, A., P., Coutinho, E. M., Silva, E. D., Ferreira, A. G. P., Miranda, P., Krieger, M. A., Goldenberg, S., Soares, M. B. P., Correa-Oliveira, R., & Gomes, Y. M. (2004). Immunization with cytoplasmic repetitive antigen and flagellar repetitive antigen of Trypanosoma cruzi stimulates a cellular immune response in mice. *Parasitology, 129*(5), 563–570. https://doi.org/10.1017/S0031182004006043.

Pérez-Vergara, L. D., Cifuentes, M. T., Franco, A. P., Pérez-Cervera, C. E., & Andrade-Pizarro, R. D. (2020). Development and characterization of edible films based on native cassava starch, beeswax, and propolis. *NFS Journal, 21*, 39–49. https://doi.org/10.1016/j.nfs.2020.09.002.

Periasamy, S., Lin, C. H., Nagarajan, B., Sankaranarayanan, N. V., Desai, U. R., & Liu, M. Y. (2018). Mucoadhesive role of tamarind xyloglucan on inflammation attenuates ulcerative colitis. *Journal of Functional Foods, 47*(January), 1–10. https://doi.org/10.1016/j.jff.2018.05.035.

Picone, P., Sabatino, M. A., Ajovalasit, A., Giacomazza, D., Dispenza, C., & Di Carlo, M. (2019). Biocompatibility, hemocompatibility and antimicrobial properties of xyloglucan-based hydrogel film for wound healing application. *International Journal of Biological Macromolecules, 121*, 784–795. https://doi.org/10.1016/j.ijbiomac.2018.10.078.

Picout, D. R., Ross-Murphy, S. B., Errington, N., & Harding, S. E. (2003). Pressure cell assisted solubilization of xyloglucans: Tamarind seed polysaccharide and detarium gum. *Biomacromolecules, 4*(3), 799–807. https://doi.org/10.1021/bm0257659.

Ramsey, D. (1995). Effects of three occlusive dressing materials on healing of full-thickness skin wounds in dogs. *American Journal of Veterinary Research, 56*(7), 941–949. PMID: 7574165.

Recalcati, S., Locati, M., & Cairo, G. (2012). Systemic and cellular consequences of macrophage control of iron metabolism. *Seminars in Immunology, 24*(6), 393–398. https://doi.org/10.1016/j.smim.2013.01.001.

Recalcati, Stefania, Gammella, E., Buratti, P., Doni, A., Anselmo, A., Locati, M., & Cairo, G. (2019). Macrophage ferroportin is essential for stromal cell proliferation in wound healing. *Haematologica, 104*(1), 47–58. https://doi.org/10.3324/haematol.2018.197517.

Rodrigues, D. C., Cunha, A. P., Silva, L. M. A., Rodrigues, T. H. S., Gallão, M. I., & Azeredo, H. M. C. (2018). Emulsion films from tamarind kernel xyloglucan and sesame seed oil by different emulsification techniques. *Food Hydrocolloids, 77*, 270–276. https://doi.org/10.1016/j.foodhyd.2017.10.003.

Santos, A. F. S., Da Silva, M. D. C., Napoleão, T. H., Paiva, P. M. G., Correia, M. T. S., & Coelho, L. C. B. B. (2014). Lectins: Function, structure, biological properties and potential applications. *Current Topics in Peptide and Protein Research, 15*(June), 41–62.

Santos, N. L., Braga, R. C., Bastos, M. S. R., Cunha, P. L. R., Mendes, F. R. S., Galvão, A. M. M. T., Bezerra, G. S., & Passos, A. A. C. (2019). Preparation and characterization of Xyloglucan films extracted from Tamarindus indica seeds for packaging cut-up 'Sunrise Solo' papaya. *International Journal of Biological Macromolecules, 132*, 1163–1175. https://doi.org/10.1016/j.ijbiomac.2019.04.044.

Serra, M. B., Barroso, W. A., Silva, N. N. Da, Silva, S. D. N., Borges, A. C. R., Abreu, I. C., & Borges, M. O. D. R. (2017). From Inflammation to Current and Alternative Therapies Involved in Wound Healing. *International Journal of Inflammation, 2017*. https://doi.org/10.1155/2017/3406215.

Shevchenko, A., Tomas, H., Havliš, J., Olsen, J. V., & Mann, M. (2007). In-gel digestion for mass spectrometric characterization of proteins and proteomes. *Nature Protocols, 1*(6), 2856–2860. https://doi.org/10.1038/nprot.2006.468.

Shivakumar, P., Gupta, M. S., Jayakumar, R., & Gowda, D. V. (2021). Prospection of chitosan and its derivatives in wound healing: Proof of patent analysis (2010–2020).

International Journal of Biological Macromolecules, 184, 701–712. https://doi.org/10.1016/j.ijbiomac.2021.06.086.

Silva, A. F. B., Matos, M. P. V., Ralph, M. T., Silva, D. L., De Alencar, N. M., Ramos, M. V., & Lima-Filho, J. V. (2016). Comparison of immunomodulatory properties of mannose-binding lectins from Canavalia brasiliensis and Cratylia argentea in a mice model of Salmonella infection. *International Immunopharmacology, 31*, 233–238. https://doi.org/10.1016/j.intimp.2015.12.036.

Silva, F., de, O., Araújo, R. V.de S., Schirato, G. V., Teixeira, E. H., Melo Júnior, M. R.de, Cavada, B.de S., Lima-Filho, J. L.de, Carneiro-Leão, A. M.dos A., & Porto, A. L. F. (2009). Perfil de proteasesde lesões cutâneas experimentais em camundongos tratadas com a lectina isolada das sementes de Canavalia brasiliensis. *Ciência Rural, 39*(6), 1808–1814. https://doi.org/10.1590/s0103-84782009000600026.

Simi, C. K., & Abraham, T. E. (2010). Biodegradable biocompatible xyloglucan films for various applications. *Colloid and Polymer Science, 288*, 297–306. https://doi.org/10.1007/s00396-009-2151-8.

Singer, A. J., & Clark, R. A. F. (1999). Epstein1999_Woundhealing. *The New England Journal of Medicine*.

Singh, B., & Pal, L. (2012). Sterculia crosslinked PVA and PVA-poly(AAm) hydrogel wound dressings for slow drug delivery: Mechanical, mucoadhesive, biocompatible and permeability properties. *Journal of the Mechanical Behavior of Biomedical Materials, 9*, 9–21. https://doi.org/10.1016/j.jmbbm.2012.01.021.

Singh, B., Sharma, S., & Dhiman, A. (2013). Design of antibiotic containing hydrogel wound dressings: Biomedical properties and histological study of wound healing. *International Journal of Pharmaceutics, 457*(1), 82–91. https://doi.org/10.1016/j.ijpharm.2013.09.028.

Siracusa, V. (2012). Food Packaging Permeability Behaviour: A Report. *International Journal of Polymer Science*, 11. https://doi.org/10.1155/2012/302029.

Souza, M. P., Vaz, A. F. M., Silva, H. D., Cerqueira, M. A., Vicente, A. A., & Carneiro-da-Cunha, M. G. (2015). Development and Characterization of an Active Chitosan-Based Film Containing Quercetin. *Food and Bioprocess Technology, 8*(11), 2183–2191. https://doi.org/10.1007/s11947-015-1580-2.

Sujja-areevatha, J., Mundaya, D. L., Coxa, P. J., & AKhan, K. A. (1998). Relationship between swelling, erosion and drug release in hydrophillic natural gum mini-matrix formulations. *European Journal of Pharmaceutical Sciences, 6*, 207–217. https://doi.org/10.1016/S0928-0987(97)00072-9.

Tottoli, E. M., Dorati, R., Genta, I., Chiesa, E., Pisani, S., & Conti, B. (2020). Skin wound healing process and new emerging technologies for skin wound care and regeneration. *Pharmaceutics, 12*(8), 1–30. https://doi.org/10.3390/pharmaceutics12080735.

Üstündağ Okur, N., Hökenek, N., Okur, M. E., Ayla, Ş., Yoltaş, A., Siafaka, P. I., & Cevher, E. (2019). An alternative approach to wound healing field; new composite films from natural polymers for mupirocin dermal delivery. *Saudi Pharmaceutical Journal, 27*(5), 738–752. https://doi.org/10.1016/j.jsps.2019.04.010.

Valenga, F., Petri, D. F. S., Lucyszyn, N., Jó, T. A., & Sierakowski, M. R. (2012). Galactomannan thin films as supports for the immobilization of Concanavalin A and/or dengue viruses. *International Journal of Biological Macromolecules, 50*(1), 88–94. https://doi.org/10.1016/j.ijbiomac.2011.10.005.

Xiao, T., Yan, Z., Xiao, S., & Xia, Y. (2020). Proinflammatory cytokines regulate epidermal stem cells in wound epithelialization. *Stem Cell Research and Therapy, 11*(1), 1–9. https://doi.org/10.1186/s13287-020-01755-y.

Yadav, H., & Maiti, S. (2020). Research progress in galactomannan-based nanomaterials: Synthesis and application. *International Journal of Biological Macromolecules, 163*, 2113–2126. https://doi.org/10.1016/j.ijbiomac.2020.09.062.

Zhang, J., Wang, C., Chen, S., Yuan, D., & Zhong, X. (2013). Amperometric glucose biosensor based on glucose oxidase-lectin biospecific interaction. *Enzyme and Microbial Technology, 52*(3), 134–140. https://doi.org/10.1016/j.enzmictec.2012.12.005.

Zhou, K., Taoerdahong, H., Bai, J., Bakasi, A., Wang, X., & Dong, C. (2020). Structural characterization and immunostimulatory activity of polysaccharides from Pyrus sinkiangensis Yu. *International Journal of Biological Macromolecules, 157*, 444–451. https://doi.org/10.1016/j.ijbiomac.2020.04.146.